The Heat and Freshwater Budgets of the Red Sea

Elina Tragou,* Chris Garrett, and Richard Outerbridge

School of Earth and Ocean Sciences, University of Victoria, Victoria, British Columbia, Canada

Craig Gilman

Department of Marine Science, Coastal Carolina University, Conway, South Carolina

ABSTRACT

The heat and freshwater transports through the Strait of Bab el Mandab, connecting the Red Sea with the open ocean, are reviewed and used to test air–sea fluxes from a revised version of the Comprehensive Ocean–Atmosphere Data Set (UWM/COADS). Using historical data for the volume fluxes and water properties, the annual-mean net heat transport through the strait is found to require an average surface heat loss of 8 ± 2 W m^{-2}, while the requirement for conservation of salt in the basin implies a net evaporation rate of 1.60 ± 0.35 m yr^{-1}, lower than previously considered. The air–sea heat fluxes from UWM/COADS overestimate the total heat flux by nearly 100 W m^{-2}; the discrepancy is attributed to systematic errors in the bulk formulas used to calculate the heat flux components. In particular, insolation appears to be overestimated by 36 W m^{-2}, largely due to the neglect of aerosols. The effect of these is determined from ground stations and satellite data on the optical thickness index. The net longwave radiation appears to be underestimated by 21 W m^{-2} or more. The latent heat flux from UWM/COADS may also be underestimated as it corresponds to an evaporation rate of 1.60 m yr^{-1}, less than the 1.75 ± 0.35 m yr^{-1} implied by the net evaporation defined from the water budget, plus an annual average precipitation rate of 0.15 m yr^{-1} from UWM/COADS. The net evaporation is the main contributor to the annual-mean buoyancy flux of approximately 2×10^{-8} m^2 s^{-3}.

1. Introduction

The Red Sea is a fascinating part of the world's oceans because of the unique physical and biogeochemical processes encountered there. It is well known as the first region where hot brines were discovered at the seafloor (Miller 1964), and where the rich geothermal and geomagnetic activity has been associated with the initial stage of oceanic floor formation due to the spreading of tectonic plates (Verzhbitskiy and Shreider 1995). Another remarkable feature of the Red Sea is that it has the highest surface salinities in the World Ocean (apart from very small lagoons), caused by the intense evaporation rate of about 2 m yr^{-1} (Morcos 1970). In response to the surface buoyancy loss there is a near-surface influx from the Gulf of Aden of fresher water, which undergoes density increase in the Red Sea, sinks,

and eventually leaves the sea through the shallow Strait of Bab el Mandab. This salty Red Sea water spreads into the Indian Ocean, much as Mediterranean Water spreads into the North Atlantic, and significantly affects the structure of the northwest Indian Ocean (Shapiro and Meschanov 1991).

The seasonally changing wind patterns at the southern end of the sea are believed to affect the buoyancy-driven circulation. In particular, the reversal of the monsoons modifies the exchange flow through the Strait of Bab el Mandab. During the winter it enhances the surface inflow of the two-layer exchange system. During the summer wind-induced upwelling in the Gulf of Aden is believed to be the main reason for the development of the observed three-layer exchange system at the Strait (Patzert 1974; Smeed 1997), with near-surface outflow, intermediate inflow of water from the Gulf of Aden, and bottom outflow of Red Sea water (Maillard and Soliman 1986).

The processes associated with the buoyancy forcing of the Red Sea have been the subject of several studies. Most of them focus on the analysis of observations or interpretation of the buoyancy and tracer budgets (e.g., Maillard and Soliman 1986; Cember 1988), while some emphasize the deep-water formation and renewal time-scales (e.g., Eshel et al. 1994; Woelk and Quadfasel

* Current affiliation: Physical Oceanography Group, Department of Applied Physics, University of Athens, Athens, Greece.

Corresponding author address: Dr. Elina Tragou, Department of Applied Physics, University of Athens, University Campus, Building PHYS-V, 157 84 Athens, Greece.
E-mail: tragou@oc.phys.uoa.gr

1996). Attempts to understand the dynamics of the thermohaline circulation have been presented recently (Eshel and Naik 1997; Maxworthy 1997; Tragou and Garrett 1997), but accurate modeling of the mainly buoyancy-driven circulation requires adequate knowledge of the air–sea fluxes.

At present there are two methods of estimating the air–sea heat fluxes: (i) the bulk formulas in conjunction with long-term marine meteorological and hydrographic observations and (ii) satellite observations. Because of the duration of datasets from voluntary observing ships, estimates from bulk formulas are still more widely used; they will be examined in this paper for their implications for the heat and freshwater budgets of the Red Sea. It is well known, however, that there are systematic errors in the formulas, or in the data, causing uncertainties even in the sign of the heat and freshwater budgets of certain areas of the World Ocean (e.g., Garrett et al. 1993; da Silva et al. 1994). Uncertainties exist in all four components of the surface heat flux, although the latent heat is considered to have a higher uncertainty than the other components (Weare 1989). Estimating the air–sea fluxes of the Red Sea is useful for the study of the buoyancy-driven circulation of the sea itself, but the semienclosed nature of the Red Sea can also be utilized to provide a check on the datasets and formulas that are used on a global scale, as has been done for the Mediterranean by Bunker et al. (1982, henceforth BCG), by Garrett et al. (1993), and by Gilman and Garrett (1994).

Patzert (1974) estimated a small net heat transport (of about 7 W m^{-2}) into the Red Sea from temperature and current measurements at the Strait of Bab el Mandab, which implies that an annual heat loss from the surface of 7 W m^{-2} must occur if the heat content of the basin is conserved. Exchanges between the Red Sea and the Mediterranean through the Suez Canal are negligible, so heat and freshwater exchanges at Bab el Mandab provide a strong constraint on the Red Sea heat and freshwater surface fluxes. However, in the first estimate of the heat fluxes of the Red Sea using data from voluntary observing ships (VOS) and bulk formulas, BCG estimated a significant surface net heat gain by the Red Sea instead of a loss. They suggested that this discrepancy might be due to an overestimation of the solar irradiance, and, more significantly, due to an underestimation of the latent heat flux because of systematic errors in the observations.

In this paper we present first a critical review of previous estimates for the heat and freshwater transports through the strait; these indicate the expected surface fluxes. Next we reexamine the estimates of individual heat flux components, using the revised Comprehensive Ocean–Atmosphere Data Set of da Silva et al. (1994) at the Department of Geoscience of the University of Wisconsin—Milwaukee (henceforth referred to as UWM/COADS), and currently accepted bulk formulas. We find a total net surface heat input, significantly higher than the original estimate of BCG, rather than a loss.

We suggest that possible explanations for this discrepancy include the role of regionally high aerosol concentration in attenuating the solar irradiance, and we explore this using optical thickness data from satellites. There also appears to have been an underestimation of the longwave back radiation, and underestimation of the latent heat flux, possibly due to an underestimation of wind speed.

2. Oceanic heat and freshwater transports through the Strait of Bab el Mandab

a. Review of annual estimates

Heat and freshwater transports through a section at the entrance of the Red Sea may be calculated from direct in situ measurements of temperature and salinity with simultaneous observations of the currents, but the results must be compatible with conservation of volume and salt (the Knudsen formulas). For the Red Sea these are

$$-\overline{F}_1 + \overline{F}_2 - \overline{F}_3 = \overline{E}_{net}A \qquad (2.1)$$

$$-\overline{\rho_1 S_1 F_1} + \overline{\rho_2 S_2 F_2} - \overline{\rho_3 S_3 F_3} = 0, \qquad (2.2)$$

where $\overline{F}_i$ ($i = 1, 2, 3$) are the annual-mean volume fluxes in Sverdrups (Sv $\equiv 10^6$ m^3 s^{-1}) of the surface outflow F_1 (present during summer months only), the intermediate (summer only) or surface inflow F_2, and the bottom outflow F_3; A is the surface area of the Red Sea (0.45 $\times$ 10^{12} m^2), and $E_{net} = E - P$, where E is the evaporation and P the precipitation (both in m s^{-1}): there is no runoff in the Red Sea. Here ρ_i and S_i are the average densities and salinities of the corresponding layers.

Monthly volume fluxes for the near-surface layer (i.e., F_1 from June to September and F_2 from October to May) have been estimated by Patzert (1974) using ship drift observations [from the Koninklijk Nederlands Meteorologisch Instituut (KNMI) Atlas (1949)], and summertime volume fluxes for the intermediate layer (F_2) are available from measurements by Maillard and Soliman (1986). These are listed in the second and third column of Table 1. Monthly mean temperature and salinity profiles are taken from Levitus et al. (1994) at the grid point closest to the strait (15.5°N, 41.5°E), but 250 km to the northwest of Bab el Mandab where the total depth is about 400 m. Since the sill is about 150 km northwest of Bab el Mandab narrows, the hydrographic data are about 100 km away from the sill. The sensitivity of our results to this effect was checked by allowing for a time lag of one month for the inflowing water to reach that point, which is the speed of propagation of the inflowing water according to Smeed (1997). No significant differences were found. The structure of the water column at this grid point shows two layers (0–100 m and 100–400 m) during the winter months (October–May), and a three-layer system (0–30 m, 30–100 m, and 100–400 m) from June to September. The monthly

Table 1. Monthly mean volume transports for the near-surface layer (F_1 from Jun to Sep and F_2 from Oct to May) from Patzert (1974), and for the intermediate layer F_2 (from Jul to Sep) from Maillard and Soliman (1986). The deep outflow F_3 is estimated from Eq. (2.1) with a monthly constant $E_{net}A$. Temperatures and salinities for the three layers near the sill are taken from Levitus et al. (1994) climatology, as is the basin-average sea surface temperature T_s. Our estimates for the monthly heat and salt transports are listed in the last two columns.

Month	F_1 (Sv)	F_2 (Sv)	F_3 (Sv)	T_1 (°C)	T_2 (°C)	T_3 (°C)	T_s (°C)	S_1 (psu)	S_2 (psu)	S_3 (psu)	F_T (W m^{-2})	F_S (10^6 kg s^{-1})
1		0.57	−0.55		25.0	22.5	25.5		37.7	40.3	12.3	−0.6
2		0.40	−0.38		24.9	22.7	25.0		37.8	40.2	7.5	−0.0
3		0.57	−0.55		25.2	22.5	25.3		37.9	40.1	13.1	−0.5
4		0.42	−0.40		26.0	22.5	26.6		38.2	40.6	12.4	−0.1
5		0.38	−0.36		26.3	22.5	28.3		38.3	40.5	12.0	0.0
6	−0.06	0.31*	−0.23	29.5	25.1	22.3	29.4	37.2	39.0	40.6	2.6	0.7
7	−0.20	0.25	−0.03	30.7	24.9	22.5	30.3	37.5	38.6	40.3	−11.1	1.1
8	−0.21	0.33	−0.10	30.9	24.2	22.4	30.8	37.8	38.0	40.4	−12.5	0.8
9	−0.09	0.20	−0.09	31.2	22.9	22.0	30.6	38.5	37.8	40.5	−7.7	0.6
10		0.52	−0.50		26.7	22.0	30.1		37.8	40.4	20.3	−0.4
11		0.57	−0.55		26.6	20.6	28.4		38.0	40.3	28.8	−0.5
12		0.51	−0.49		25.9	22.1	26.7		37.7	40.4	16.2	−0.5

* Interpolated from the F_2 transports in May (Patzert 1974) and July (Maillard and Soliman 1986).

mean values for T_i and S_i averaged over each layer are listed in Table 1.

Evaporation rates for the Red Sea have been estimated by Yegorov (1950) (2.30 m yr^{-1}), Neumann (1952) (2.15 m yr^{-1}), and Privett (1959) (1.83 m yr^{-1}) using a bulk formula for the water vapor transfer, as described by Morcos (1970) in his thorough review of the Red Sea. There are considerable differences among these estimates not only for the annual rate but also in the seasonality; Privett reports a higher evaporation rate during winter, while Yegorov and Neumann found maximum evaporation rates during summer.

To provide an estimate for the evaporation rate that would satisfy the Knudsen formulas, we consider both $\overline{E}_{net}$ and $\overline{F}_3$ as unknowns and solve the system of equations (2.1) and (2.2). This gives the annual-mean $\overline{E}_{net}$ = 1.60 ± 0.35 m yr^{-1}, smaller than previously claimed. The overall uncertainty is estimated from the ±20% uncertainty in the volume flux and ±10% uncertainty in the salinity differences between inflow and outflow. The latter is estimated from the average deviation of the salinity difference from the smoothed annual cycle of the salinity difference with a fifth-degree polynomial fit. A similar estimate of $\overline{E}_{net}$ using the same climatological salinities and updated volume fluxes for the lower layer F_3 from Murray and Johns (1997), and considering F_2 as unknown, also gave $\overline{E}_{net}$ = 1.60 m yr^{-1}.

The estimated monthly $\overline{E}_{net}$ (assumed constant) balances the monthly volume budget (2.1) to provide the unknown volume transport F_3 (seasonal changes in the evaporation rate and volume changes due to sea level changes are neglected), so that we may estimate the annual-mean heat transport $\overline{F}_T$. This is expressed as the equivalent flux across the surface of the Red Sea and is estimated from the formula

$$\overline{F}_T = \frac{1}{A}\rho c_p(-\overline{F_1 T_1} + \overline{F_2 T_2} - \overline{F_3 T_3} - A\overline{E_{net}T_s}), \quad (2.3)$$

where ρ is the mean water density (1025 kg m^{-3}), c_p is the heat capacity of water (3986 J K^{-1} kg^{-1}), and T_i are the mean temperatures of the inflowing and outflowing layers. The last term in Eq. (2.3) represents the heat transport due to the volume that leaves the basin through its surface and it should be included when $\Sigma F_i \neq 0$; otherwise the net heat transport at the strait depends on the choice of temperature scale (i.e., Celsius or kelvin). The temperature of the evaporated volume of water is the sea surface temperature, therefore we have used the monthly mean temperature climatology from UWM/COADS for T_s combined with the annual evaporation rate $E_{net}A$ of 0.023 Sv to estimate the net heat transport $\overline{F}_T$ as approximately 8 ± 2 W m^{-2} (the uncertainty in the temperature differences between inflow and outflow is 10%). This compares well with the original estimate by Patzert (1974) of 7 W m^{-2}, who used historical monthly temperature profiles from the National Oceanographic Data Center (NODC) combined with the aforementioned monthly volume transports from KNMI. Our monthly estimates for the heat transport are listed in Table 1 and plotted in Fig. 1a. We note that, in principle, the last term in Eq. (2.3) should be $-EAT_s + PAT_p$ where P is the rate and T_p the temperature of the precipitation, but the effect of this is negligible. The monthly heat transport estimated from Eq. (2.3) is rather insensitive to uncertainty and seasonal changes in E_{net} so that use of the annual average E_{net} in (2.3) is adequate.

Our estimates for the monthly salt transports are listed in Table 1 and plotted in Fig. 1b. While we have assumed a monthly constant net volume flux, the salt transport from $F_S = -\rho_1 S_1 F_1 + \rho_2 S_2 F_2 - \rho_3 S_3 F_3$ allows for a monthly salt transport. The annual-mean $\overline{F}_S$ is zero.

A second estimate of the annual heat exchange through the strait was provided by Ahmad and Sultan (1989), who used the same hydrological dataset as Patz-
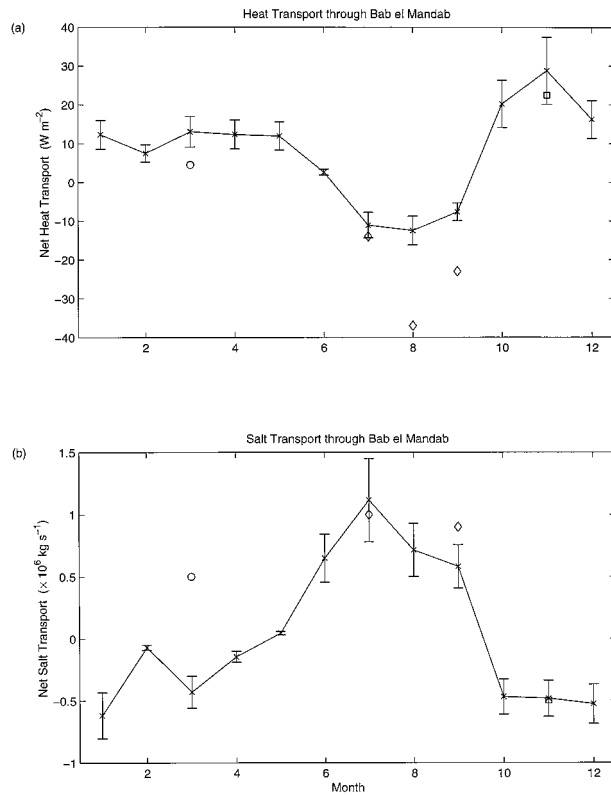
FIG. 1. Estimates of heat and salt advected through the Strait of Bab el Mandab. Crosses mark results using Patzert's volume transport, circles mark Vercelli's results, diamonds mark Maillard and Soliman's, and squares mark Siedler's. The annual-mean heat transport is equivalent to a surface heating of the Red Sea of 8 W m^{-2}. The annual-mean salt transport is zero.

ert, but unfortunately, the source of their volume flux data was not clearly stated in their paper, which makes comparison with Patzert's results difficult. The most striking difference between the two analyses is that, according to Ahmad and Sultan, the Red Sea gains heat through the strait during the summer instead of losing it as suggested by Patzert's original results (-17 W m^{-2}). Ahmad and Sultan attributed this discrepancy to Patzert's neglect of the third bottom layer carrying water out of the Red Sea, although an estimate of the summer

heat transport we carried out using Maillard and Soliman's volume fluxes, allowing for three layers, also results in a net loss of heat of -10 W m^{-2} averaged over the summer months.

Ahmad and Sultan (1989) estimated the annual average input of heat through the strait as equivalent to 19 W m^{-2} using the formula

$$F_T = \frac{1}{A}\rho c_p(F_{in}T_{in} - F_{out}T_{out}). \qquad (2.4)$$

The above formula is commonly used for heat transport calculations, although it is inappropriate when $F_{in} \neq F_{out}$ (the result is sensitive to the temperature scale). As mentioned previously, the problem can be avoided if we take into account the heat transport due to the water leaving the sea from its surface. If this amount of around 6 W m^{-2} is deducted from Ahmad and Sultan's estimate, their annual heat input is reduced to 13 W m^{-2}, closer to our result.

b. Review of seasonal estimates

Other estimates of the volume transport through Bab el Mandab have been carried out using limited time series of simultaneous current data and water properties. These include:

(a) Vercelli's volume transport estimates, based on current measurements from 15 days during March 1924 (*Arimondi* cruise). Observations during this cruise for volume flux, temperature, and salinity (Vercelli 1927) are presented in Table 2. As pointed out by Morcos (1970) and Patzert (1974), the difference of 0.09 Sv between the volume transports of the surface and subsurface layers is unlikely to be due to evaporation and sea level rise; the annual-mean evaporation rate is estimated around 0.023 Sv, and the maximum seasonal sea level change, according to Patzert's analysis, can be as high as 0.30 m leading to an equivalent volume transport of 0.01 Sv. A volume transport compatible with the measured evaporation rate is possible, if we assume that either the transport of the inflowing or outflowing layer is correct and adjust the other so that $F_{in} - F_{out} = E_{net}A = 0.023$ Sv.

The results of these adjustments are presented in Ta-

TABLE 2. Mean volume transports, temperatures, and salinities of the two-layer exchange system during Mar 1924 (Vercelli 1927), and the resulting heat and salt transports, adjusting the volume transport of the outflowing layer (upper) and inflowing layer (lower).

	F_i (Sv)	T_i (°C)	S_i (psu)	F_T (W m^{-2})	F_S (10^6 kg s^{-1})
Inflowing layer	0.58 (observed)	26.3	36.56	135	21
Outflowing layer	-0.56 (adjusted)	25.3	37.43	-125	-21
Evaporated water	-0.02	25.3		-5	
Heat and salt transports				5	0
Inflowing layer	0.51 (adjusted)	26.3	36.56	119	19
Outflowing layer	-0.49 (observed)	25.3	37.43	-110	-18
Evaporated water	-0.02	25.3		-5	
Heat and salt transports				4	1

TABLE 3. Volume transports, temperatures, and salinities of the three-layer exchange system during summer 1982 (Maillard and Soliman 1986; Souvermezoglou et al. 1989), and the estimated heat and salt transports.

		F_i (Sv)	T_i (°C)	S_i (psu)	F_T (W m^{-2})	F_S (10^6 kg s^{-1})
Jul	Surface outflow	−0.16	23.7	36.6	−34	−5.8
	Subsurface inflow	0.25	18.6	36.3	41	9.1
	Bottom outflow	−0.06	25.3	38.9	−13	−2.3
	Evaporated water	−0.03	30.3		−8	
	Heat and salt transports				−14	1.0
Aug	Surface outflow	−0.25	30.9		−70	
	Subsurface inflow	0.33	16.8		49	
	Bottom outflow	−0.05	15.9		−7	
	Evaporated water	−0.03	30.8		−9	
	Heat transport				−37	
Sep	Surface outflow	−0.14	31.2	36.6	−40	−5.1
	Subsurface inflow	0.20	17.1	35.9	30	7.2
	Bottom outflow	−0.03	16.0	38.6	−4	−1.2
	Evaporated water	−0.03	30.6		−9	
	Heat and salt transports				−23	0.9

ble 2, and we will assume that the value of heat and salt transport lies somewhere between the two results. The calculation of the heat flux due to evaporated water was done using the mean sea surface temperature during March given by UWM/COADS. We have ignored the volume difference caused by the sea level rise during winter, but this is expected to introduce a small error compared to the uncertainties of the volume transports at the strait.

(b) Maillard and Soliman (1986) estimated the volume fluxes through Bab el Mandab using current meter observations obtained during the summer (July–September) of 1982 (*Marion Dufresne* cruise). Although a problem with the instrumentation allowed for measurements only of the intermediate and bottom layer properties, one may still get an estimate of the heat transport using monthly mean temperatures at the surface layer from the Levitus climatology for August and September. No salinity records are available for August. The volume fluxes for the surface and bottom layers in their study are estimated from the volume budget taking $E_{net}A = 0.03$ Sv, and also with their assumption that there is a proportionality between the volume transports and the

corresponding areas A_1 and A_2 of the cross sections such that $F_1/F_3 = A_1/A_3$. The data from this cruise along with the salt transport analyzed by Souvermezoglou et al. (1989), and our estimates of the heat transport are presented in Table 3. We note that the water properties measured during that cruise are significantly different from the climatological values we have used in Table 1. In particular, the temperatures and salinities of the bottom outflow are very low, but we have included these estimates for completeness.

(c) Siedler (1968) used a very short time series of observations during two and a half days of November 1964 (*Meteor* cruise) to estimate the volume transports through the strait. His estimates for volume transport are presented in Table 4. The difference between the inflow and outflow is 0.16 Sv, five times larger than the measured difference due to evaporation! An adjustment of the volume transports to match the observed evaporation rate, similar to that applied to Vercelli's measurements, has been used in order to estimate the heat and salt transports implied by Siedler's volume transports, and the results are presented in Table 4. Climatological data (Levitus et al. 1994) for the temperature

TABLE 4. Mean volume transports during Nov 1964 from Siedler (1968), and estimates of heat and salt transport using climatological temperatures and salinities (Levitus et al. 1994), adjusting the volume transport of the outflowing layer (upper) and inflowing layer (lower).

	F_i (Sv)	T_i (°C)	S_i (psu)	F_T (W m^{-2})	F_S (10^6 kg s^{-1})
Inflowing layer	0.58 (observed)	26.6	38.02	136	22
Outflowing layer	−0.56 (adjusted)	20.6	40.33	−102	−23
Evaporated water	−0.02	28.4		−8	
Heat and salt transports				26	−1
Inflowing layer	0.44 (adjusted)	26.6	38.02	103	17
Outflowing layer	−0.42 (observed)	20.6	40.33	−76	−17
Evaporated water	−0.02	28.4		−8	
Heat and salt transports				19	0

and salinity of the two layers were used in our calculations.

Figure 1a shows all the above results for the heat budget and Fig. 1b the salt budget, and how they compare to each other. The monthly heat transport using volume transport from Patzert has an annual average of approximately 8 W m^{-2} and compares well with the short-time observations except during late summer; the heat loss in August and September is stronger with Maillard and Soliman's records. The seasonal cycle shows that the maximum transport of heat to the Red Sea occurs during the fall, while there is heat loss during the summer months. The annual average salt transport is zero and its seasonal cycle shows that there is a gain of salt during the summer and a loss during the winter, in agreement with the estimates of Souvermezoglou et al. (1989) with an inverse model. We note that the uncertainties of the salt transports with data from Vercelli (1927) and Siedler (1968) are $\pm 0.5 \times 10^6$ kg s^{-1}, same size as the estimated values.

Observations of temperature, salinity, and currents at Bab el Mandab were also presented by Jones et al. (1974) and Van Aken and Otto (1974) for two experiments conducted during September 1971 and March 1967, respectively. Calculations of the heat and freshwater transport were not provided by either of the two studies. Jones et al. (1974) argued that during their three-week experiment the currents show high variability, and, although the current meters suggest a two-layer exchange system, the vertical distributions of temperature and salinity show a three-layer system. Still, an estimate of the heat exchange would have been possible if the bottom topography at the current meter station was known. Estimation of the heat and freshwater transport using the one-day data of Van Aken and Otto (1974) is not possible as their current meter station was located in a shallow area of the Strait and only one layer of the exchange system is captured, suggesting outflow at all depths.

It is evident that the exchange at Bab el Mandab is not accurately measured and that more simultaneous in situ records of currents and water properties in the vicinity of Bab el Mandab are needed to estimate the annual heat and salt transports of the Red Sea. Some results of such a project were presented by Murray and Johns (1997) and the complete analysis of their data should shed more light on the physics of the strait. At any rate, if there is a small temperature difference between the inflow and the colder outflow [of about 2°C (Smeed 1997)], a typical outflow of 0.4 Sv would give an equivalent surface heat loss of about 7 W m^{-2}. It is unlikely, therefore, that updated measurements will dramatically upset the present picture of the heat budget of the Red Sea. For the freshwater budget, however, updated simultaneous records for the salinity and volume fluxes are indeed a necessity and will hopefully narrow the large error bounds of the currently known values.

For the moment, based on the above analysis, we believe that the volume exchange through Bab el Mandab suggests that the sea is experiencing net cooling through its surface at a small rate (of approximately 8 $\pm$ 2 W m^{-2}) while the freshwater transport is equivalent to an annual average net evaporation rate of 1.60 ± 0.35 m yr^{-1}. We have not considered the interannual variability of these fluxes, though this may be significant.

3. Surface heat flux estimates

BCG first used a dataset of meteorological observations, made from VOS for the years 1941–72, to calculate the surface heat fluxes for the Mediterranean and the Red Sea. Their initial results using bulk formulas for the heat flux components of the Red Sea were

$$\overline{Q}_s - \overline{Q}_b - \overline{Q}_e - \overline{Q}_h = \overline{Q}_t,$$

$$263 - 76 - 135 - 5 = +47 \text{ W m}^{-2},$$

where Q_s is the solar irradiance, Q_b the net longwave radiation, Q_e the latent heat flux, Q_h the sensible heat flux, and Q_t the total heat flux. An overbar denotes the annual and basin average. BCG recognized that there may be considerable errors in the radiative fluxes Q_s and Q_b and pointed out the increased aerosol concentration of the Red Sea region as a likely cause for reducing the possibly overestimated insolation. They preferred, however, to attribute the large difference between the estimated $\overline{Q}_t$ and the expected small heat loss to an underestimated latent heat flux caused by the fact that they used monthly mean winds and temperature and humidity differences rather than their monthly mean products, as well as systematic errors in observations of meteorological parameters (wind, temperature, and humidity); they mentioned that such errors may include ship's flow distortion and avoidance of high winds, although the latter seems implausible for the narrow Red Sea. Nevertheless, BCG tried to account for these biases by significantly increasing the exchange coefficients for latent and sensible heat fluxes. This gave

$$263 - 76 - 183 - 3 = +1 \text{ W m}^{-2},$$

in better agreement with the oceanic heat flux through the strait. Apart from the known biases on the wind speed scale (e.g., Kaufeld 1981), however, there has been no confirmation for such an increase of the value of the exchange coefficients. In addition, as we will discuss later, such an arbitrary increase of the latent heat flux may not be consistent with the water budget of the basin, as was pointed out by Garrett et al. (1993) for the Mediterranean.

Ahmad and Sultan (1989) used meteorological data from three coastal stations and four near-coast stations on the east coast of the Red Sea, taken during the period 1970–85, to obtain

$$210 - 66 - 169 + 3 = -22 \text{ W m}^{-2}.$$

The negative $\overline{Q}_t$ is in quantitative agreement with the observed advected heat flux, although the net heat loss through the sea surface is higher than the expected -8 W m^{-2}. This is partly due to the relatively low insolation (obtained from inland stations where the effect of aerosols is expected to significantly attenuate the solar radiation), and partly because the latent and sensible heat fluxes were estimated with the increased exchange coefficients suggested by BCG.

An up-to-date estimate of the total heat flux is also possible by extracting the estimates for the four heat flux components over the Red Sea from the global dataset UWM/COADS of da Silva et al. (1994, henceforth dSYL). This dataset covers the 45-yr period from January 1945 to December 1989 and comes from the initial COADS release (Woodruff et al. 1987) objectively analyzed on a $1° \times 1°$ global grid. The dataset includes corrections to the wind speed, cloud cover, and present weather (PW) observations, as well as global estimates for the four components of the heat budget evaluated using standard bulk formulas, and estimates for the freshwater and buoyancy fluxes. From the UWM/COADS the heat fluxes averaged over 45 years and over the Red Sea give

$$272 - 55 - 129 - 5 = +83 \text{ W m}^{-2},$$

which is very far from the expected small negative $\overline{Q}_t$. The same dataset contains data for the constrained net heat and freshwater fluxes that are compatible with meridional global balances at 65°S (0 PW for the heat and 0.06 Sv for the freshwater transports). Unfortunately, even the constrained net heat flux yields

$$250 - 57 - 146 - 5 = +42 \text{ W m}^{-2}$$

for the Red Sea.

In the following sections we have reexamined each component of the heat budget separately, using meteorological parameters from the recent UWM/COADS and commonly used bulk formulas, in an attempt to find an explanation for the discrepancy between the heat flux at the strait and the surface heat budget.

a. Solar irradiance

The insolation Q_s at the sea surface was calculated by dSYL using the commonly used formula

$$Q_s = Q_{CS}(1 - c_n n + 0.0019h)(1 - \alpha). \quad (3.1)$$

This is a combination of the cloud reduction formula from Reed (1977) and the formula for the clear sky irradiance Q_{CS} from List (1958). The latter comes from the sum of direct and scattered solar radiation as given by Rosati and Miyakoda (1988). This is

$$Q_{CS} = \frac{1}{2}Q_0(\text{Tr}^{1/\cos z} + (1 - A)), \quad (3.2)$$

where Q_0 is the incident radiation at the top of the atmosphere ($Q_0 = S_0 \cos z$, with $S_0 = 1370$ W m^{-2} the

solar constant, and z the solar zenith angle), Tr is the transmission factor for a clear atmosphere (held constant at 0.7), and $A = 0.09$ is the absorption factor due to ozone and water vapor. In Eq. (3.1) the reduction due to clouds is parameterized, following Reed (1977), by the product of the cloud fraction n and a coefficient $c_n = 0.62$; h is the noon solar altitude in degrees and α is the albedo of the sea surface taken from Payne (1972).

The Red Sea average of $\overline{Q}_s$, calculated from dSYL with Eq. (3.1) and the cloud cover fraction from UWM/COADS, is 272 W m^{-2}. However, when the cloud cover fraction n is smaller than about 0.2 the calculated solar radiation Q_s from Eq. (3.1) is larger than the clear sky irradiance Q_{CS} and an overestimation of Q_s is introduced. Therefore, as pointed out by Reed (1977), the cloud reduction formula should be truncated at 1. For example, in the Mediterranean Gilman and Garrett (1994) found that correct usage of Reed's formula reduces the Q_s by 4 W m^{-2}. Moreover, the cloudiness from UWM/COADS includes some small negative values, mainly during the period 1967–75, presumably stemming from extrapolations in the objective analysis. To correct for these effects we apply the Reed cloud reduction only when it gives $Q_s < Q_{CS}$, and otherwise set $Q_s = Q_{CS}$. This correction gives $\overline{Q}_s = 264$ W m^{-2}, which is a 3% (8 W m^{-2}) reduction in $\overline{Q}_s$ for the Red Sea.

The spatial distribution of the corrected annual-mean insolation $\overline{Q}_s$ is shown in Fig. 2, and the seasonal variability of the spatial mean Q_s is shown later in Fig. 6a. It should be noted that there is a clear north–south gradient in $\overline{Q}_s$ (changing by 7%) with higher $\overline{Q}_s$ values at the southern end.

da Silva et al. (1994) also carried out an inverse calculation for the global heat fluxes, to match certain global constraints. They provided tuning parameters for the heat flux components, though they provided no physical justification. The correcting factors for the insolation formula are 0.92 (on the clear sky radiation) and 1.04 (on the cloudiness coefficient), so that Eq. (3.1) becomes

$$Q_{s_{\text{dSYL}}} = 0.92Q_{CS}(1 - 1.04c_n n + 0.0019h)(1 - \alpha). \quad (3.3)$$

The mean Red Sea insolation obtained using the above formula is 250 W m^{-2}.

Another independent estimate for the solar irradiance of the Red Sea comes from the dataset of Bishop et al. (1997). They have calculated the global Q_s for an 8-yr period (July 1983–June 1991) using data from the International Satellite Cloud Climatology Project (ISCCP) and a revised algorithm of Bishop and Rossow (1991). The surface solar irradiance from this dataset (denoted $Q_{s_{\text{BR2}}}$) gives an average of 273 W m^{-2} over the Red Sea. All of the above $\overline{Q}_s$ estimates are listed in Table 5 (the last entry will be discussed shortly).

For the Mediterranean insolation Gilman and Garrett (1994) showed that there is a systematic error in the parameterization of atmospheric attenuation in the for-
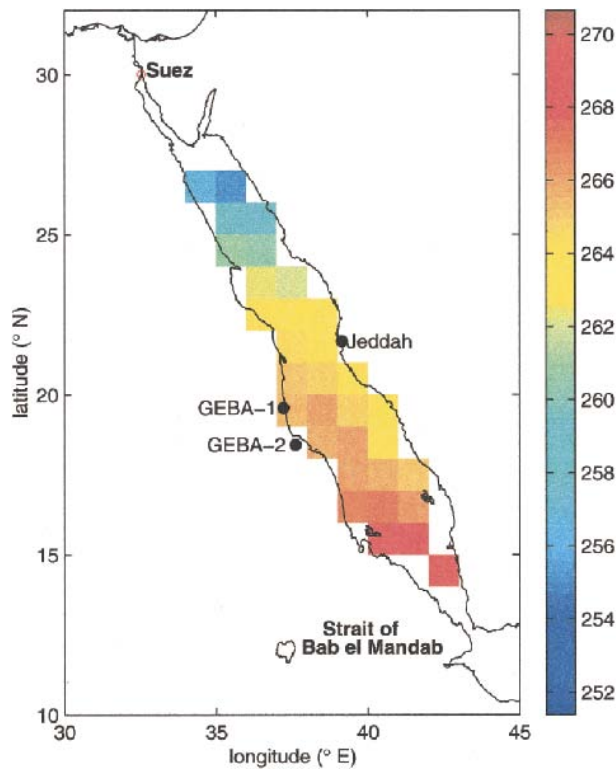
FIG. 2. Long-term averaged net shortwave solar radiation Q_s estimated from Eq. (3.1) (with the cloud correction) and cloudiness from UWM/COADS.

mula for the solar irradiance. Indeed, the transmission coefficient in formula (3.1) is assumed spatially and temporally constant and a value of 0.7 is commonly used to parameterize the extinction due to absorption and scattering by aerosols and other atmospheric constituents such as water vapor, ozone, CO_2, etc. However, concentrations of natural and anthropogenic aerosols may vary both in space and time so that the parameterization of aerosol effects as constant can lead to significant errors in estimating the insolation. In particular, the Red Sea appears to be within a dusty environment due to anthropogenic and, particularly, mineral aerosols. This is evident from the global distributions of the index of aerosol optical thickness detected by polar orbiting satellites [Advanced Very High Resolution Radiometer (AVHRR) data] over the oceans presented by Husar et al. (1997), who also showed that there is significant seasonal variability of the aerosol concentration in the

atmosphere. Unfortunately, the currently available index of aerosol optical thickness cannot be simply related to the transmission coefficient Tr of clear sky insolation because the data do not provide information about aerosol properties (i.e., size, shape, and composition), and lack the required calibration (Lacis and Mishchenko 1995).

Nevertheless, monthly data for insolation from coastal stations can be compared to Q_s obtained from the bulk formula (3.1), with the cloud correction, to estimate a factor that will be assumed to represent the attenuation due to aerosols. The results of this comparison can be used in an attempt to calibrate satellite data so that we can obtain a picture of the spatial variability of the effect of aerosols throughout the Red Sea.

Observations of surface solar irradiance from the Global Energy Balance Archives (GEBA) are available for two coastal stations on the west coast of the Red Sea (Ohmura and Gligen 1991). These include monthly mean measurements of Q_s from July 1983 to August 1985 for the locations marked GEBA-1 and GEBA-2 in Fig. 2. Ground-truth observations are also available for a station at Jeddah, Saudi Arabia (Fig. 2), on the central east coast of the Red Sea, in the form of monthly averages of Q_s for the period 1980–85 (Ahmad et al. 1989).

The monthly solar irradiance at the three stations according to the ground-truth measurements and the estimates from Eq. (3.1) are presented in Fig. 3. The observed values (solid circles) are, in general, lower than the estimated Q_s values (crosses), and the minimum insolation is observed at Jeddah. We note, however, that the ground measurements at GEBA-1 are very irregular and include values higher than the Q_s estimates.

Bishop et al. (1997) compared the globally estimated $Q_{s_{BR2}}$ using their revised algorithm and data from the ISCCP, with ground-truth data from globally scattered GEBA stations $Q_{s_{GEBA}}$. In this algorithm the effect of aerosols was held constant in space and time. Therefore, in order to bring the calculated surface solar irradiance into agreement with surface observations, they have estimated the optical extinction anomaly τ^* defined from

$$\frac{Q_{s_{GEBA}}}{Q_{s_{BR2}}} = \exp(-\tau^*/\cos z^*), \quad (3.4)$$

where $Q_{s_{GEBA}}$ is the monthly averaged solar irradiance measured at the ground stations GEBA, $Q_{s_{BR2}}$ is the monthly solar irradiance from Bishop et al. (1997) av-

TABLE 5. List of estimates for the mean surface solar radiation of the Red Sea.

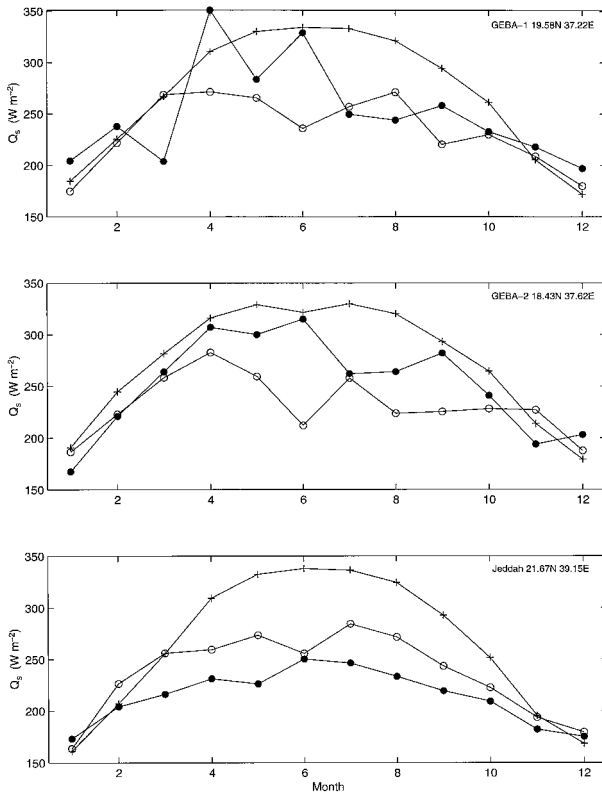| Reference	Method	Dataset	$\overline{Q}_s$ (W m^{-2})
Bishop et al. (1997)	Bishop and Rossow (1991) algorithm	ISCCP	273
da Silva et al. (1994)	Bulk formula (3.1)	UWM/COADS	272
this study	Bulk formula (3.1) with cloud correction	UWM/COADS	264
da Silva et al. (1994)	Bulk formula (3.3)	UWM/COADS	250
this study	Bulk formula (3.1) with cloud and aerosol correction	UWM/COADS	236

FIG. 3. Net shortwave radiation at three stations. Crosses mark the estimated Q_s from Eq. (3.1) (with the cloud correction), solid circles mark the observed Q_s, and open circles mark the corrected Q_s using the transmission anomaly Tr* from satellite data calibrated to ground stations.

eraged over the 8-yr period July 1983 to June 1991 (the resolution is $2.5° \times 2.5°$ and has been interpolated to the position of the ground stations), and $\cos z^*$ is the flux-weighted cosine of solar zenith angle.

Alternatively, Eq. (3.4) also defines a transmission coefficient anomaly Tr* due to the neglect (or underestimation) of the effect of aerosols in Eq. (3.2) by using a spatially and temporally constant Tr. The transmission coefficient anomaly Tr* is defined by comparing the ground measurements Q_{s_G} with the insolation estimated with Eq. (3.1) for the same period of time

$$\frac{Q_{s_G}}{Q_s} = \text{Tr*}, \qquad (3.5)$$

where Q_{s_G} is the monthly mean insolation at the two stations from GEBA and the one at Jeddah. The resulting transmission anomaly coefficient for the three stations in the central Red Sea is shown in Fig. 4a along with the mean of Tr* from GEBA and Jeddah and a smoothed version of this. It should be noted that there is a strong seasonal signal in the anomaly, with a 25% difference between summer and winter months.

The transmission factor Tr* calculated with the above procedure can be used to calibrate satellite data for the index of optical thickness in order to obtain the spatial variability of Tr*. These data include monthly observations for the aerosol optical thickness index τ_s^A derived for the ocean from NOAA AVHRR data on a $1° \times 1°$ resolution for the period from July 1989 to June 1991 (Stowe et al. 1997) and they have been averaged to obtain the seasonal cycle. In the method of derivation
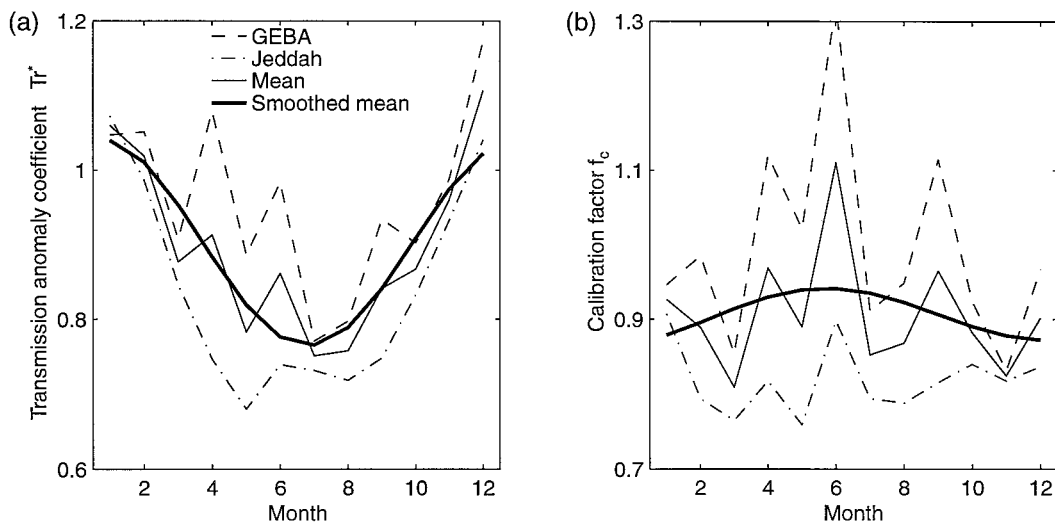

FIG. 4. (a) Transmission anomaly coefficient estimated from comparison of the insolation at ground-truth stations with the calculated Q_s (with the cloud correction) during the same period of time (Tr* $= Q_{s_G}/Q_s$). The dashed line is the mean Tr* from the GEBA stations, the dashed–dotted line is Tr* from the station at Jeddah, the solid line is the average between the results at GEBA and Jeddah (assuming 50% weights to GEBA and Jeddah, i.e., 25% to each GEBA station and 50% to Jeddah). The thick solid line is the smoothed average Tr*. The smoothing is obtained with a 10th-order polynomial fit on three repetitive annual cycles of the mean Tr* and keeping the second annual cycle. (b) Calibration factor for the satellite transmission coefficient index estimated from comparison of the insolation from satellite data with the ground-truth records; the line style corresponds to that of (a).
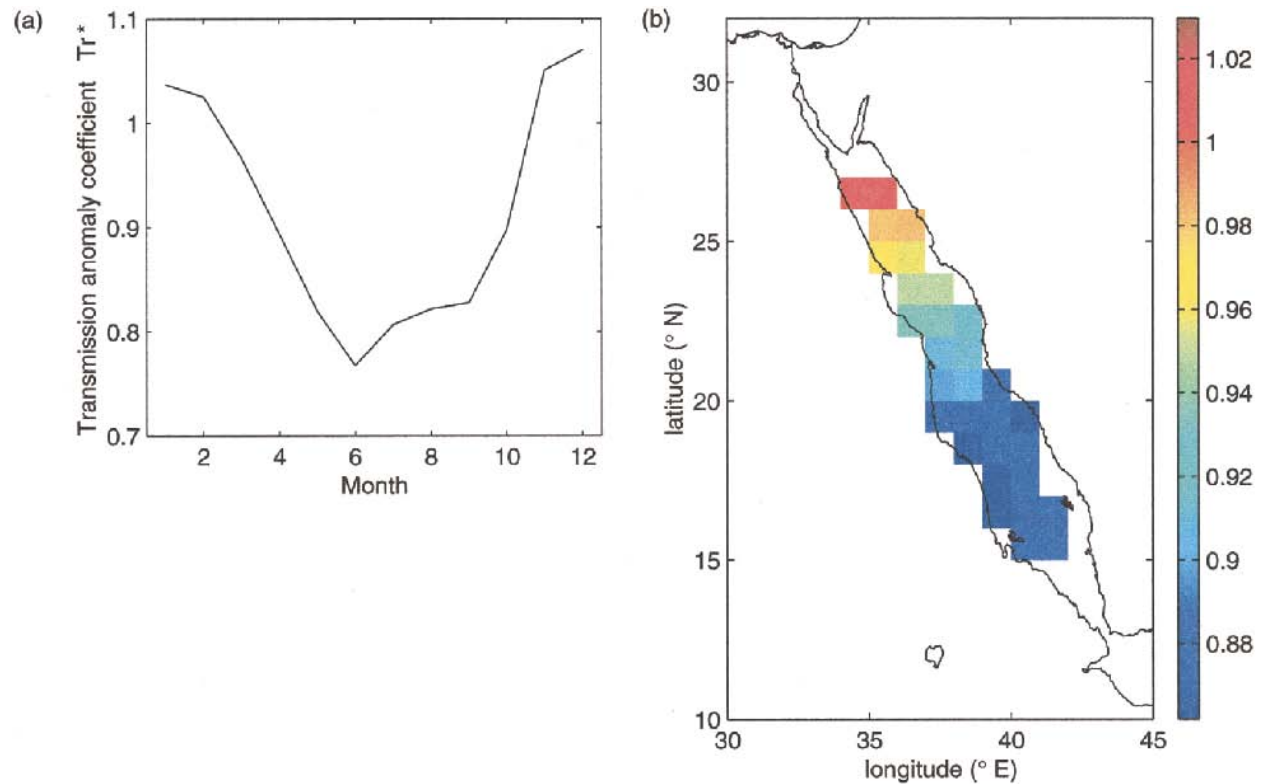
FIG. 5. Transmission anomaly coefficient Tr* for the Red Sea from the optical extinction index calibrated to ground observations: (a) seasonal cycle and (b) geographical distribution.

of τ_s^A, aerosols are assumed to be purely scattering. We assume that the satellite data for the index τ_s^A define a transmission coefficient $Tr_s^A = \exp(-\tau_s^A/\cos z)$ due to aerosol scattering. We also introduce a coefficient f_c for the attenuation of Q_0 due to absorption and scattering by atmospheric molecules and absorption by aerosols so that the clear sky insolation at the sea surface is given by $Q_0 f_c Tr_s^A$.

Combining Eqs. (3.1), (3.2), and (3.5), and assuming that the transmission anomaly coefficient Tr* is solely due to errors in the estimation of Q_{CS}, the clear sky insolation at the coastal stations is given by $Q_0 f Tr^*$, where $f = \frac{1}{2}[Tr^{1/\cos z} + (1 - A)]$. To calibrate the clear sky insolation from the satellite data to the measured clear sky insolation, the coefficient f_c has to be adjusted so that

$$f_c = f \frac{Tr^*}{Tr_s^A}. \qquad (3.6)$$

At GEBA and Jeddah stations the calibration factor f_c is evaluated using the average monthly values of Tr*, the monthly aerosol transmission coefficient Tr_s^A (at grid points nearest to the coastal stations), and the monthly values of the parameter f. The seasonal cycle of f_c for GEBA, and Jeddah, the mean f_c, and the smoothed f_c are shown in Fig. 4b. We note that the calibration factor f_c includes all the corrections required to match Q_{CS}

from satellite data to the measured quantity at ground stations. These include the attenuation of Q_0 due to absorption and scattering by atmospheric molecules, aerosol absorption, as well as errors in Tr_s^A.

We have used this seasonally varying but spatially constant calibration factor f_c and the seasonal value of f to estimate the transmission coefficient anomaly

$$Tr^* = \frac{f_c}{f} Tr_s^A,$$

using the satellite aerosol transmission coefficient Tr_s^A everywhere in the Red Sea. Figure 5a shows that there is strong seasonality of the basin-averaged Tr* with a seasonal change of around 25%. Figure 5a also suggests that there is some underestimation of the insolation during winter months (Tr* > 1), while there is significant overestimation during summer. From the spatial distribution of the annual-mean Tr* (Fig. 5b), it is evident that there is a north–south gradient implying that Q_s is overestimated toward the southern end of the Red Sea.

This spatially and seasonally varying transmission coefficient Tr* is multiplied by the surface solar irradiance obtained with Eq. (3.1) including the cloud correction. The resulting corrected $Q_{s_C} = Tr^* Q_s$ is presented in Fig. 6. Figure 6a shows the seasonal cycle of the 45-yr average of Q_{s_C}. We note that there is a reduction of 28 W m^{-2} (or 11%) from the initial $\overline{Q}_s = 264$ W m^{-2}, pre-
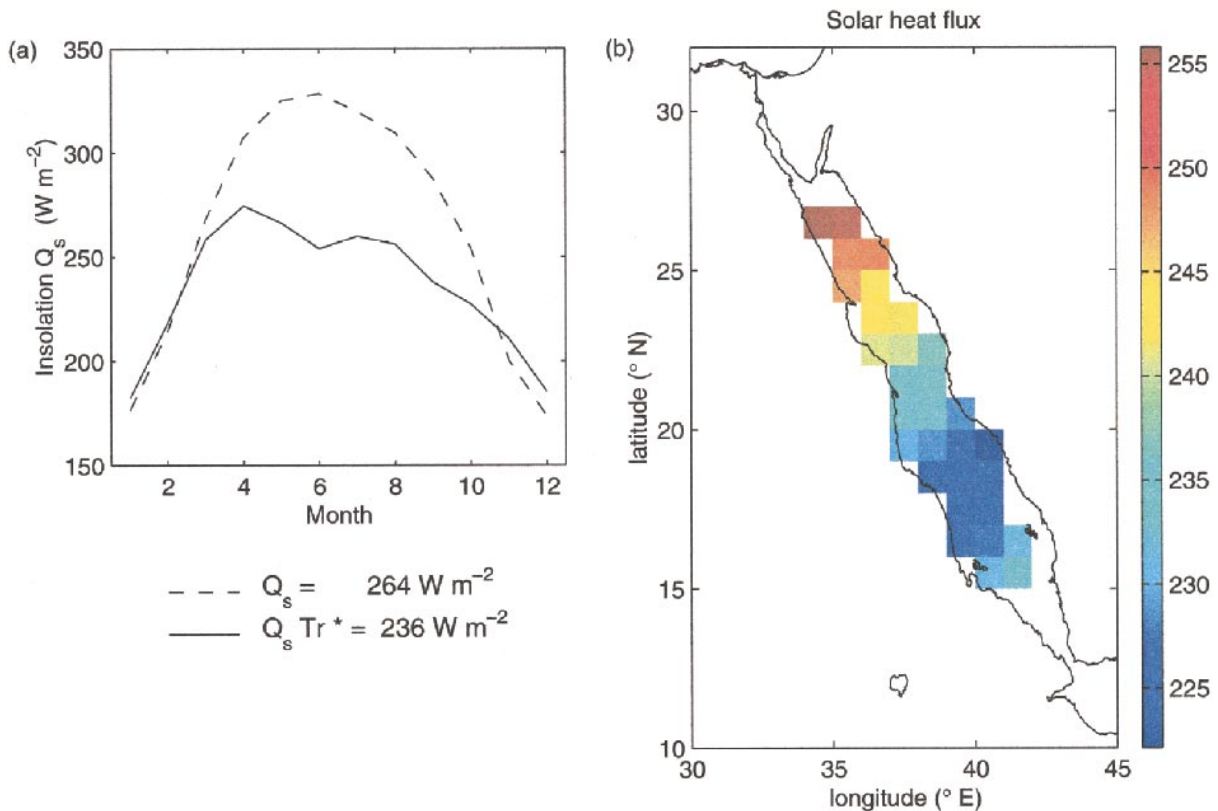
FIG. 6. Insolation corrected for the attenuation due to aerosols: (a) seasonal cycle and (b) spatial distribution.

sumably because of the effect of aerosols on the insolation. Figure 6b shows the spatial distribution of the mean Q_{sc}. Comparison of Fig. 6b with Fig. 2 shows that the north–south gradient is now reversed and the higher insolation occurs toward the northern end of the Red Sea because of the higher aerosol concentration at the southern end. The reversal of the geographical gradient in insolation cannot be verified by ground stations as the available data come from the central Red Sea area.

The basin-averaged 45-yr mean $\overline{Q}_{sc}$ is listed in Table 5 and the monthly values of the corrected Q_{sc} at the ground stations are plotted in Fig. 3.

b. Longwave radiation

The net longwave radiation at the sea surface is the result of emission, absorption, and scattering in the atmospheric column, and so depends on the concentrations of atmospheric constituents and the vertical distribution of temperature, humidity, and cloud properties. Since direct measurements of the net longwave radiation at the ocean surface are sparse, it has become common to derive Q_b with the aid of various bulk formulas or, more recently, with a radiative transfer model (e.g., Zhang et al. 1995).

The bulk formulas assume that the surface properties

of temperature and humidity represent those of the atmospheric column, and they introduce various parameterization schemes with constants derived from regression fitting to certain sets of observations. In general, only the cloud fraction is taken into consideration and the cloud type (high, medium, or low) is ignored, thus increasing the uncertainty of the calculations (Fung et al. 1984). Thus one cannot expect very accurate estimates from the bulk formulas. Bulk formulas are still widely used, however, because they allow the computation of Q_b from routinely measured parameters such as sea surface temperature, air temperature, the water vapor pressure near the sea surface, and cloudiness.

In Table 6 we present estimates of the 45-yr mean net longwave radiation calculated using three different bulk formulas and data for sea temperature, air temperature, vapor pressure, and cloud fraction from UWM/COADS. The formula of Berland and Berland (1952) was used by dSYL in their calculation of Q_b. However, a comparison of the mean $\overline{Q}_b$ for the Mediterranean carried out by Gilman and Garrett (1994) suggested that this formula significantly underestimates Q_b there. We have calculated $\overline{Q}_b$ using the formula introduced by Bunker and Goldsmith (1979), which is the only bulk formula that allows for the effect of a seasonally prescribed mix of low, medium, and high cloud type. Data for the cloud type in the Red Sea were provided by R.

TABLE 6. List of methods used to calculate net longwave radiation, and the annual Red Sea estimates using various datasets.

Reference	Method	Dataset	$\overline{Q}_b$ (W m^{-2})
da Silva et al. (1994)*	$\epsilon\sigma T_s^4 (0.39 - 0.05e^{1/2})(1 - \chi c^2) + \epsilon\sigma T_s^3 (T_s - T_a)$	UWM/COADS	55
Bunker and Goldsmith (1979)	Bunker (1976) formula—seasonal mix of cloud type	UWM/COADS	73
Bignami et al. (1995)	$\epsilon\sigma T_s^4 - \sigma T_a^4 (0.653 + 0.00535e)(1 + 0.1762c^2)$	UWM/COADS	76
Rossow and Zhang (1995)	Radiative Transfer Model	ISCCP	104

* Based on Berliand and Berliand (1952): $\epsilon = 0.98$ is the sea surface emissivity; $\sigma = 5.6697 \times 10^{-8}$ W m^{-2} K^{-4} is the Stefan–Boltzmann constant; T_s, T_a are the sea surface and air temperatures; e is the near sea surface water vapor pressure in hPa; c is the cloud cover fraction; χ is a coefficient varying with latitude.

Goldsmith. The mean $\overline{Q}_b$ we found using the Bunker and Goldsmith formula is 73 W m^{-2}, while BCG estimated 76 W m^{-2}.

More recently, Bignami et al. (1995) proposed another formula with constants calculated from regression to measurements of longwave radiation in the Western Mediterranean. This formula is the first strictly derived from marine data. They compared the observations in the Mediterranean with results from previous formulas and found that the latter systematically underestimate longwave radiation by approximately 30 W m^{-2}. Josey et al. (1997) found that the Bignami et al. formula performs best in semienclosed seas rather than open ocean conditions where other formulas [such as Clark et al. (1974)] are more appropriate. We have tested the Bignami et al. formula in the Red Sea (assuming that the relations between surface parameters and atmospheric profiles are similar to those of the Mediterranean) and found a value of 76 W m^{-2}, close to the result using the formula of Bunker and Goldsmith (1979).

We have also compared the results of the bulk formulas with Q_b estimates extracted from a global dataset for radiative fluxes, evaluated using a radiative transfer model and data from ISCCP (during the period April 1985–January 1989) by Rossow and Zhang (1995). The mean value of $\overline{Q}_b$ over the Red Sea area is 104 W m^{-2} though uncertainties in the calculation reach 15 W m^{-2}. The source of these uncertainties in subtropical regions is equally distributed between uncertainties in cloud properties, and atmospheric and surface water properties. It should be emphasized that $\overline{Q}_b$ from the radiative transfer model is significantly larger than that from the bulk formulas and the uncertainty of the former cannot account for the difference. We note, however, that the resolution of the Rossow and Zhang (1995) dataset is $2.5° \times 2.5°$, which is very coarse for the narrow Red Sea and it is very likely that the extracted annual-mean Q_b is more representative of the surrounding land rather than the Red Sea itself. Therefore we will consider the $\overline{Q}_b = 76$ W m^{-2} found with the Bignami et al. (1995) formula as our best estimate for the longwave radiation.

c. Latent and sensible heat fluxes

Latent and sensible heat fluxes are, in general, given by the formulas

$$Q_e = \rho c_p L C_e (q_s - q)W \tag{3.7}$$

$$Q_h = \rho c_p C_h (T_s - T_a)W, \tag{3.8}$$

with ρ the air density determined from atmospheric pressure and air temperature, c_p the specific heat of air, and L the latent heat of evaporation. Also, q_s is the saturation humidity at the sea surface temperature, q the observed specific humidity, T_s and T_a are the sea surface and air temperatures, and W the wind speed; C_e and C_h are exchange coefficients.

As mentioned previously, BCG used large values for C_e and C_h ($C_e = C_h = 2.1 \times 10^{-3}$), compared to those deduced from measurements, to account for the discrepancy of the total heat budget. Such an increase could compensate for the fact that they used monthly mean winds and temperature and humidity differences rather than their monthly mean products, as well as for substantial systematic uncertainties in the observations, particularly the wind speed. The same high coefficients were used by Ahmad and Sultan (1989).

Da Silva et al. estimated C_e and C_h following the method of Large and Pond (1982), which gives numbers very close to those suggested by Smith (1988, 1989). According to this method, both of the exchange coefficients are functions of wind speed, air temperature, and its difference from sea surface temperature, and the difference of saturation humidity at the sea surface from the specific humidity. In neutral conditions C_e has a value of 1.2×10^{-3}, and C_h is around 1.2×10^{-3} for unstable stratification and 0.75×10^{-3} for stable stratification. The basin-averaged 45-yr mean $\overline{Q}_e$ and $\overline{Q}_h$ extracted from dSYL's dataset are 129 W m^{-2} and 5 W m^{-2}, respectively.

The mean $\overline{Q}_e$ and $\overline{Q}_h$ from the above studies are listed in Table 7 along with the exchange coefficients in neutral conditions. The last entry will be discussed shortly. Very large differences (up to 40%) exist between the quoted $\overline{Q}_e$ values, indicative of the uncertainty of this heat flux component. However, $\overline{Q}_e$ can be constrained by the water budget of the basin, which is examined next.

d. Implications from the water budget

In section 2a we provided an estimate for the net annual-mean evaporation rate of $\overline{E}_{net} = 1.60 \pm 0.35$ m

TABLE 7. List of exchange coefficients (in neutral conditions) used to calculate latent and sensible heat fluxes and their mean values in the Red Sea.

Reference	$C_e \times 10^{-3}$	$C_h \times 10^{-3}$	$\overline{Q}_e$ (W m^{-2})	$\overline{Q}_h$ (W m^{-2})
Bunker et al. (1982)	2.1	2.1	183	3
Ahmad and Sultan (1989)	2.1	2.1	169	−3
da Silva et al. (1994)	1.2	1.2	129	5
da Silva et al. (1994) corrected	1.3	1.2	146	5

yr^{-1}, using the constraint of zero salt flux through the strait. From this estimate we may infer the annual-mean evaporation $\overline{E}$ = 1.75 ± 0.35 m yr^{-1} assuming an annual-mean precipitation rate of $\overline{P}$ = 0.15 m yr^{-1} from the UWM/COADS climatology. Since the evaporation rate is related to the latent heat flux as $E = Q_e/\rho L$, the estimated annual-mean $\overline{E}$ corresponds to an annual-mean $\overline{Q}_e$ = 140 ± 28 W m^{-2}. The $\overline{Q}_e$ values estimated by BCG and Ahmad and Sultan (1989), listed in Table 7, are too large to satisfy the water budget constraint, as a consequence of using an excessively high exchange coefficient C_e. The $\overline{Q}_e$ value from dSYL falls within the limits of the constraint, although it is closer to the lower end.

For the calculation of the latent heat flux dSYL used corrected data for the wind speed. This correction was applied on a global basis to reduce the bias associated with an erroneous Beaufort equivalent scale that causes underestimated climatological wind speeds. This effect appears as a trend in the long-term time series as the proportionality of wind speeds estimated from sea state versus speeds measured from anemometer changes. The correction, based on a regression formula, has been applied to those data flagged as estimated, and according to dSYL has reduced the trend.

The Red Sea averaged time series for the wind speed (Fig. 7a), however, shows that there is still a remarkable trend in the wind, particularly during the last two decades, which is transferred to the estimated latent heat
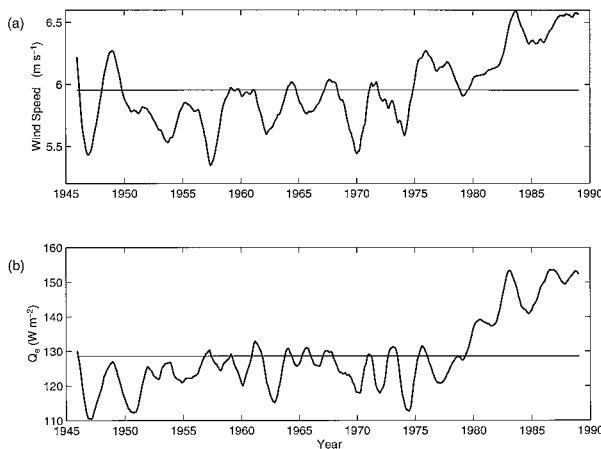

FIG. 7. (a) Monthly mean wind speed averaged over the Red Sea and filtered with a 23-point filter to remove seasonal variability. (b) Latent heat flux estimated from UWM/COADS.

flux (Fig. 7b). This may be caused by limitations of the dSYL method [such as the assumption that all anemometer measurements are made at 20-m height, or due to falsely flagged data (Kent and Taylor 1997)]. If the trend in the wind speed is unrealistic and results in an underestimation of the winds in the Red Sea, it may provide an explanation for the relatively low latent heat flux compared to the expected value from the water budget constraint.

We note that in their inverse calculation, dSYL suggested a correction factor of 1.13 for C_e and 1.02 for C_h. They ascribed this correction to the uncertainties in the calculation of the exchange coefficients, implying even higher C_e and C_h than those suggested by Large and Pond (1982). We suggest that for the Red Sea the correction to the exchange coefficients could be related to underestimated winds rather than underestimated exchange coefficients. Using dSYL's correction parameters the mean latent heat flux is $\overline{Q}_e$ = 146 W m^{-2}, very close to the value inferred from the water budget. The sensible heat flux is again $\overline{Q}_h$ = 5 W m^{-2} (Table 7).

e. Total heat flux

The heat flux components averaged over the Red Sea according to the initial calculations of dSYL in the World Ocean gave

$$\overline{Q}_s - \overline{Q}_b - \overline{Q}_e - \overline{Q}_h = \overline{Q}_t$$

$$272 - 55 - 129 - 5 = +83 \text{ W m}^{-2}.$$

We have found an overestimate of $\overline{Q}_s$, due to two separate processes, amounting to 36 W m^{-2}. The net longwave radiation was reestimated with a new formula from Bignami et al. (1995), which gave $\overline{Q}_b$ = 76 W m^{-2}. The latent heat flux appears low compared to the value of 140 W m^{-2} suggested by the water budget, although the uncertainty is very large (up to 39 W m^{-2}). Further increase of the coefficient C_e seems physically implausible, but the persistent trend in the wind speeds may be the reason for the low $\overline{Q}_e$ values. With the above corrections, the total heat fluxes are

$$236 - 76 - 140 - 5 = +15 \text{ W m}^{-2}$$

so that the original discrepancy from the expected negative $\overline{Q}_t$ of −8 ± 2 W m^{-2} is reduced by 75%. The remaining difference could be due to an overestimation of $\overline{Q}_s$ or, more likely, due to an underestimation of $\overline{Q}_b$
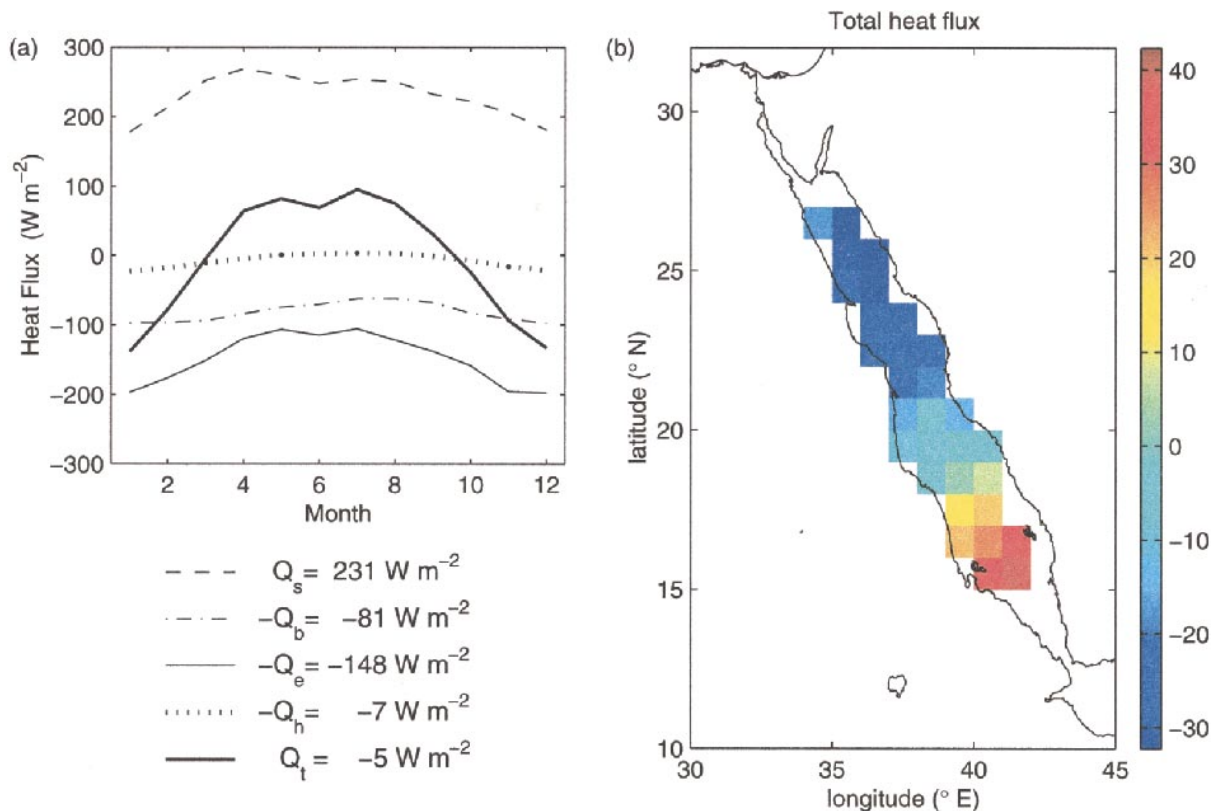
FIG. 8. (a) Seasonal cycle of the heat flux components; the dashed line is the insolation, the dash–dotted line is the net longwave radiation, the thin solid line is the latent heat flux, the dotted line is the sensible heat flux, and the thick solid line is the total heat flux. (b) Spatial distribution of the total heat flux $\overline{Q}_t$.

since a large further increase of $\overline{Q}_e$ would result in inconsistency with the currently known water budget.

It should be emphasized, however, that considerable uncertainties exist in all four heat flux components. Since the number of observations used for the estimate of the long-term averages is $O(3 \times 10^5)$, random errors become insignificant and the total uncertainty for each heat flux estimate is only due to systematic errors in the observations and the bulk formulas parameterization. Following the error analysis of Gilman and Garrett (1994) the uncertainties for the heat flux components are $\Delta\overline{Q}_s = \pm 10$ W m^{-2} (allowing for an extra ± 5 W m^{-2} uncertainty introduced by the transmission anomaly coefficient), $\Delta\overline{Q}_b = \pm 10$ W m^{-2}, $\Delta\overline{Q}_e = \pm 15$ W m^{-2}, and $\Delta\overline{Q}_h = \pm 4$ W m^{-2}. The uncertainty in the total heat flux is ± 21 W m^{-2}. If we consider a change in each individual component only 50% of its uncertainty, we obtain our suggested budget

$$231 - 81 - 148 - 7 = -5 \text{ W m}^{-2}.$$

While this is just a guess, an independent estimate from an inverse model would give a similar result.

The seasonal cycle of the four heat flux components is shown in Fig. 8a. We note that seasonality is mostly determined by the insolation and latent heat flux, and that the total heat flux becomes negative during the winter. Figure 8b shows the long-term average geographical distribution of the total heat flux. There is a remarkable gradient in the heat flux of the basin, which loses heat in its northern end and gains heat in the southern end. The 45-yr time series (filtered for the seasonal cycle) of the four heat flux components and the total are shown in Fig. 9. The total heat flux mainly follows the interannual variability of the latent heat flux, whereas Q_s and Q_b appear to be relatively stable. We also note that there is a probably unrealistic trend in Q_t similar to the trend of Q_e, and that Q_t is mostly positive before 1977 but becomes negative from 1977 to 1989.

f. Buoyancy flux

Finally, we provide an estimate for the surface buoyancy flux, as this is the important quantity for driving the thermohaline circulation of the Red Sea. The surface buoyancy flux is given by

$$B_0 = -c_w^{-1} g\alpha Q_t + \rho_0^{-1} g\beta S(E - P) = B_{0T} + B_{0S},$$
$$(3.9)$$

where c_w is the specific heat of water, g the acceleration due to gravity, $\alpha = -\rho^{-1}(\partial\rho/\partial T)_{p,S}$ the coefficient of expansion of water at fixed pressure and salinity, and $\beta S = \rho^{-1} S(\partial\rho/\partial S)_{p,T}$. Positive B_0 values correspond to
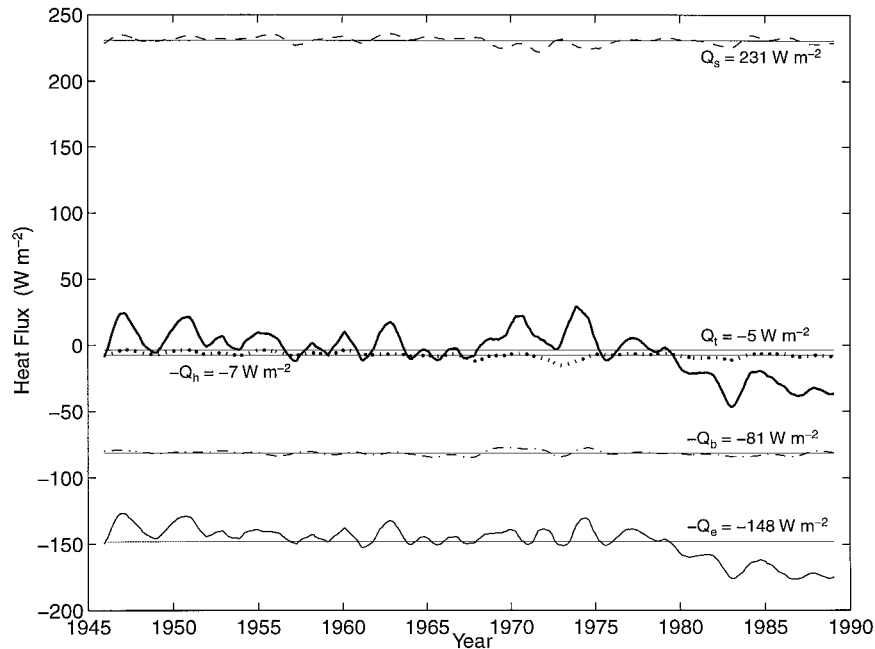
FIG. 9. Time series of the heat flux components; the line style corresponds to that of Fig. 8a.

buoyancy loss by the ocean, and B_{0T} and B_{0S} are the thermal and haline contributions.

The long-term average thermal buoyancy flux is estimated from

$$\overline{B}_{0T} = -c_w^{-1} g(\overline{\alpha}\,\overline{Q}_t + \overline{\alpha' Q'_t})$$

$$= (6.0 - 4.1) \times 10^{-6} \text{ kg m}^{-1} \text{ s}^{-3}$$

$$= 1.9 \times 10^{-6} \text{ kg m}^{-1} \text{ s}^{-3} \qquad (3.10)$$

using the adjusted total heat flux ($\overline{Q}_t = -8$ W m^{-2}) that matches the heat budget at the strait. The nonlinearity of the equation of state gives rise to the second term of Eq. (3.10), which is comparable to the first term, and is compensated by cabbeling or densification on mixing (Garrett et al. 1993). It should be emphasized, however, that forcing a model that uses buoyancy as a variable, with the total buoyancy flux B_0, including the second term of Eq. (3.10), would produce a false buoyancy input (Zahariev and Garrett 1997).

The long-term average haline buoyancy flux is

$$\overline{B}_{0S} = \rho_0^{-1} g\beta S(\overline{E} - \overline{P})$$

$$= (15.8 - 1.3) \times 10^{-6} \text{ kg m}^{-1} \text{ s}^{-3}$$

$$= 14.5 \times 10^{-6} \text{ kg m}^{-1} \text{ s}^{-3}, \qquad (3.11)$$

where $\overline{E} = 1.75$ m yr^{-1} is the evaporation rate estimated in section 3d and $\overline{P} = 0.15$ m yr^{-1} from the UWM/COADS climatology.

We conclude that the total mean surface buoyancy flux of the Red Sea is $\overline{B}_0 = 20.5 \times 10^{-6}$ kg m^{-3} s^{-3}, ignoring the correlation term ($-c_w^{-1}g\overline{\alpha' Q'_t}$) that would produce spurious buoyancy flux. This value is in accord

with our estimate of the buoyancy flux through the strait using the water properties, as was done in section 2 for the heat and freshwater fluxes. The total surface buoyancy flux is dominated by the haline term and, in particular, the evaporation; precipitation is very small and including it changes the buoyancy budget by less than 7%. Cooling plays a secondary role in the long-term mean buoyancy flux (due to its small annual-mean value), although it is dominant on seasonal timescales. We also note that the interannual variability of B_0 is determined by the thermal term, which in turn is determined by the evaporation via the latent heat flux (Fig. 9). There is buoyancy loss during most of the 45-yr period with a few, short, periods of small buoyancy gain, which are unlikely to upset the thermohaline cell of the Red Sea. The spatial distribution of the mean total buoyancy flux and its thermal and haline components are shown in Fig. 10. Spatial changes in the total buoyancy flux are controlled by the thermal component, while the haline component determines the basin-averaged value.

4. Summary and discussion

Our interest in the heat and freshwater budgets of the Red Sea is twofold: first, they allow discussion of the reliability of parameterization schemes and datasets (such as the UWM/COADS) used globally to determine surface fluxes and, second, because they provide information about the main driving force of the basin.

The total heat and freshwater transports through the Strait of Bab el Mandab provide a strong constraint for the surface fluxes. Our review of the existing obser-
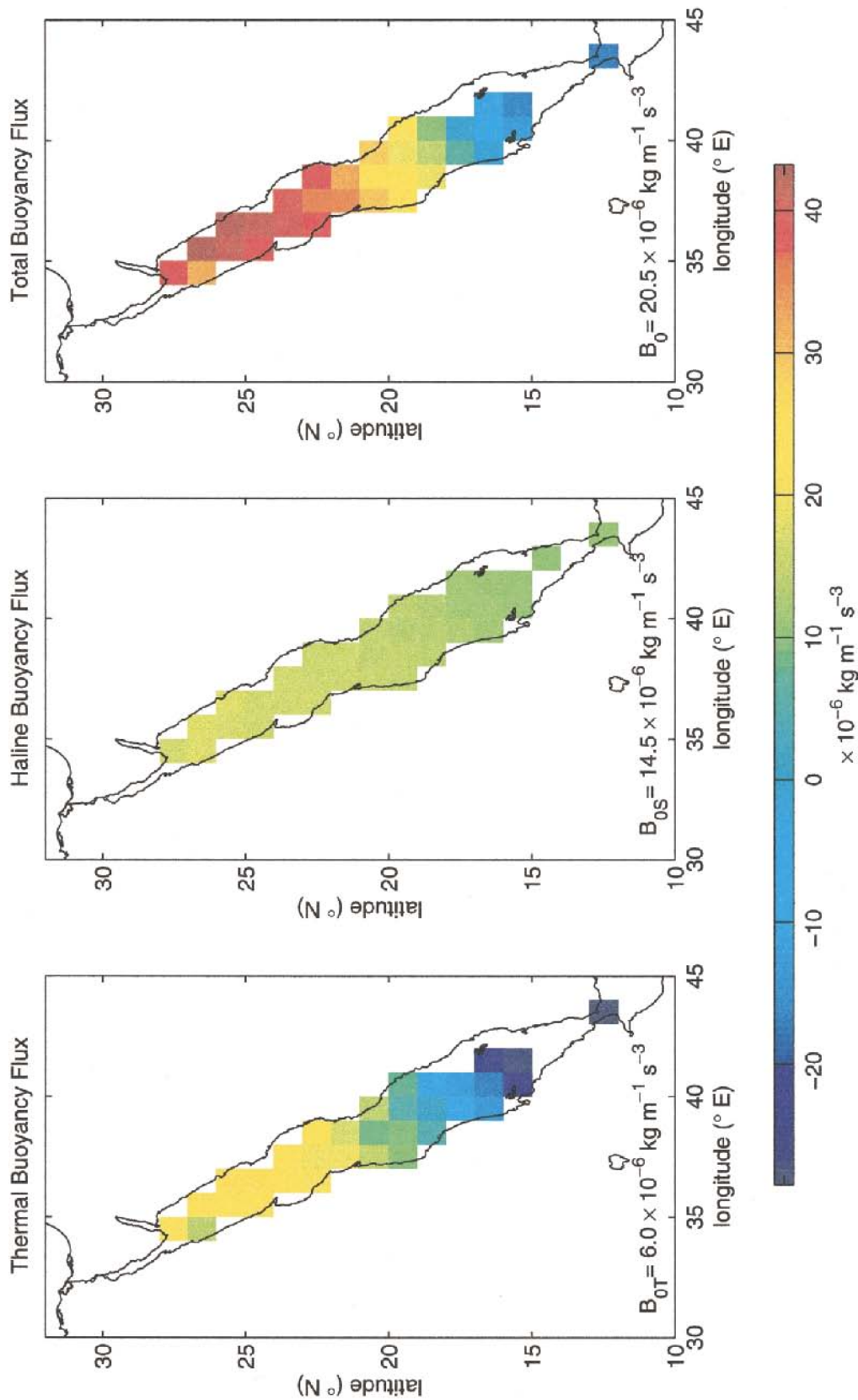
FIG. 10. Spatial distribution of the mean surface buoyancy flux: (a) thermal buoyancy flux, (b) haline buoyancy flux, and (c) total surface buoyancy flux.

vations showed that there is an annual heat transport equivalent to a surface heat flux of -8 ± 2 W m^{-2}, and the conservation of volume and salt allowed for a new estimate of the net evaporation rate of $\overline{E} - \overline{P} = 1.60 \pm 0.35$ m yr^{-1}. When combined with the UWM/COADS estimated $\overline{P} = 0.15$ m yr^{-1}, the evaporation rate is $\overline{E} = 1.75$ m yr^{-1}, lower than previously considered.

UWM/COADS contains measured and derived quantities for the air–sea exchanges, which are very important for climate studies and climate change. For the Red Sea, however, the 45-yr average total surface heat flux (estimated using standard formulas) appears to be in error, compared to the heat exchange at the Strait of Bab el Mandab, by almost 100 W m^{-2}. We suggest that a significant part of the discrepancy comes from the overestimated insolation. The remaining difference appears to be due to the underestimated net longwave radiation and latent heat flux; the sensible heat flux plays a minor role.

More specifically, the bulk formula used globally to calculate the insolation does not appear to perform well in the Red Sea as indicated by ground-truth measurements; spatial and seasonal variations of the transmission coefficient may become significant in areas of high aerosol load. We have applied a correction for this effect using satellite data calibrated to ground-truth records. We note, however, that the inverse estimate of dSYL gave a considerable reduction for Q_s close to our estimate for the dust-laden area of the Red Sea. This implies that insolation has been reduced uniformly even in areas under ''clear'' atmospheric conditions, which may introduce an error in the heat flux estimates for those areas.

Several uncertainties can be identified in our correction to Q_s: The insolation has been multiplied by a transmission anomaly estimated using observations from the period 1980–85 and the monthly means were used to calibrate the transmission coefficient calculated from satellite data during just the three years 1989–91. The monthly means from this calibration were used to correct the long-term insolation. These approximations were introduced because of the paucity of ground-truth records for the insolation available in the Red Sea, but the weak interannual variability of Q_s justifies our approach. At any rate, these observations show that there is significant overestimation of Q_s by the bulk formula widely used.

For the estimation of Q_b it seems that application of one single bulk formula on a global scale is a source of errors. Since the available bulk formulas are derived for certain atmospheric conditions, it is unlikely that they can produce reliable results everywhere in the World Ocean. We have used the formula from Bignami et al. (1995), which was derived from marine data in the Mediterranean. It is not certain, however, that the same conditions in the atmospheric column apply in the Red Sea, but there are no marine observations for the longwave radiation in the Red Sea, which would allow

comparison with the results of bulk formulas or the radiative transfer model.

Regarding the estimation of Q_e, we have pointed out that it has to be compatible with the water budget. The latent heat flux obtained from UWM/COADS appears to be underestimated compared to the evaporative loss implied by the water budget, although the uncertainties of the latter reach 28 W m^{-2}. A likely cause for the underestimation is the remaining trend in the wind speed, particularly during the last two decades. However, Kent and Taylor (1997) found that dSYL's Beaufort equivalent scale is satisfactory for the global dataset. In addition, winds higher than average and drier conditions during the last decade are in qualitative agreement with the trend in the North Atlantic Oscillation index analyzed by Hurrell (1995), but there is no similarity in the previous decades.

By applying certain corrections to Q_s, Q_b, and Q_e we have reduced the originally estimated error in Q_t by 75%. There is still a difference of 23 W m^{-2} from the expected value of $\overline{Q}_t = -8 \pm 2$ W m^{-2}, but this can be justified by only 50% of the uncertainty of each heat flux component. We emphasize that the total uncertainty in Q_t was inadequate to account for the original discrepancy of 100 W m^{-2}.

We conclude from this study that the annual-mean thermohaline circulation of the Red Sea is forced mainly by net evaporation; the thermal forcing is of secondary importance on long timescales. Because the surface heat flux is small it is well constrained in value by heat fluxes through Bab el Mandab, whereas the water budget of the basin is sensitive to uncertainty in the volume fluxes through the strait. Further measurements of these volume fluxes, combined with rainfall estimates and the requirement for conservation of salt, would allow a more accurate estimate of the average evaporation rate over the basin. This would also improve the estimate of the latent heat loss from the sea and clarify the heat budget. The interannual variability of surface fluxes in the Red Sea and exchange through the strait remains unexplored but is likely to be significant.

REFERENCES

Ahmad, F., and S. A. R. Sultan, 1989: Surface heat fluxes and their comparison with the oceanic heat flow in the Red Sea. *Oceanol. Acta,* **12,** 33–36.

——, ——, and M. O. Moammar, 1989: Monthly variations of net heat flux at the air–sea interface in coastal waters near Jeddah, Red Sea. *Atmos.–Ocean,* **27,** 406–413.

Berliand, M. E., and T. G. Berliand, 1952: Measurement of the effective radiation of the earth with varying cloud amounts (in Russian). *Izv. Akad. Nauk. SSSR, Ser. Geofiz.,* **1**.

Bignami, F., S. Marullo, R. Santoleri, and M. E. Schiano, 1995: Longwave radiation budget in the Mediterranean Sea. *J. Geophys. Res.,* **100,** 2501–2514.

Bishop, J. K. B., and W. B. Rossow, 1991: Spatial and temporal variability of global surface solar irradiance. *J. Geophys. Res.,* **96,** 16 839–16 858.

——, ——, and E. G. Dutton, 1997: Surface solar irradiance from the International Satellite Cloud Climatology Project 1983–1991. *J. Geophys. Res.,* **102** (D6), 6883–6910.

Bunker, A. F., 1976: Computation of surface energy flux and annual air–sea cycle of the North Atlantic Ocean. *Mon. Wea. Rev.,* **104,** 1122–1140.

——, and R. A. Goldsmith, 1979: Archived time-series of Atlantic Ocean meteorological variables and surface fluxes. Tech. Rep. WHOI 79-3, 28 pp. [Available from Woods Hole Oceanographic Institute, Woods Hole, MA 02543.]

——, H. Charnock, and R. A. Goldsmith, 1982: A note on the heat balance of the Mediterranean and Red Seas. *J. Mar. Res.,* **40,** 73–84.

Cember, R. P., 1988: On the sources, formation and circulation of Red Sea deep water. *J. Geophys. Res.,* **93** (C7), 8175–8191.

Clark, N. E., L. Eber, R. M. Laurs, J. A. Renner, and J. F. T. Saur, 1974: Heat exchange between ocean and atmosphere in the eastern North Pacific for 1961–71. NOAA Tech. Rep. NMFS SSRF-682, 108 pp.

da Silva, A. M., C. C. Young, and S. Levitus, 1994: *Atlas of Surface Marine Data 1994.* NOAA Atlases NESDIS 6–10, U.S. Govt. Printing Office, 5 volumes.

Eshel, G., and N. H. Naik, 1997: Climatological coastal jet collision, intermediate water formation, and the general circulation of the Red Sea. *J. Phys. Oceanogr.,* **27,** 1233–1257.

——, M. A. Cane, and M. B. Blumenthal, 1994: Modes of subsurface, intermediate, and deep water renewal in the Red Sea. *J. Geophys. Res.,* **99** (C8), 15 941–15 952.

Fung, I. Y., D. E. Harrison, and A. A. Lacis, 1984: On the variability of the net longwave radiation at the ocean surface. *J. Geophys. Res.,* **22** (2), 177–193.

Garrett, C., R. A. M. Outerbridge, and K. Thomson, 1993: Interannual variability in Mediterranean heat and freshwater fluxes. *J. Climate,* **6,** 900–910.

Gilman, C., and C. Garrett, 1994: Heat flux parameterizations for the Mediterranean Sea: The role of atmospheric aerosols and constraints from the water budget. *J. Geophys. Res.,* **99** (C3), 5119–5134.

Hurrell, J. W., 1995: Decadal trends in the North Atlantic Oscillation: Regional temperatures and precipitation. *Science,* **269,** 676–679.

Husar, R. B., J. M. Prospero, and L. L. Stowe, 1997: Characterization of tropospheric aerosols over the oceans with the NOAA advanced very high resolution radiometer optical thickness operational product. *J. Geophys. Res.,* **102,** 16 889–16 909.

Jones, E. N., J. M. Gorman, and D. G. Browning, 1974: Circulation between the Red Sea and the Gulf of Aden in late summer. *Symp. L'Oceanographie Physique de la Mer Rouge,* Paris, France, Association Internationale des Sciences Physiques de l'Ocean, 203–225.

Josey, S. A., D. Oakley, and R. W. Pascal, 1997: On estimating the atmospheric longwave flux at the ocean surface from ship meteorological reports. *J. Geophys. Res.,* **102** (C13),27 961–27 972.

Kaufeld, L., 1981: The development of a new Beaufort equivalent scale. *Meteor. Rundsch.,* **34,** 17–23.

Kent, E. C., and P. K. Taylor, 1997: Choice of a Beaufort equivalent scale. *J. Atmos. Oceanic Technol,* **14,** 228–242.

Koninklijk Nederlands Meteorologisch Instituut, 1949: Red Sea and

Gulf of Aden oceanographic and meteorological data. Publ. 129, KNMI, de Bilt, Netherlands, 26 pp.

Lacis, A. A., and M. I. Mishchencko, 1995: Climate forcing, climate sensitivity, and climate response: A radiative modeling perspective on atmospheric aerosols. *Aerosol Forcing of Climate,* R. J. Charlson and J. Heintzenberg, Eds., John Wiley, 11–42.

Large, W., and S. Pond, 1982: Sensible and latent heat flux measurements over the ocean. *J. Phys. Oceanogr.,* **12,** 464–482.

Levitus, S., R. Burgett, and T. Boyer, 1994: *World Ocean Atlas 1994.* Vol. 3: *Salinity.* NOAA Atlas NESDIS 3, 99 pp.

List, R. J., 1958: *Smithsonian Meteorological Tables.* 6th ed. Smithsonian Institution Press, 527 pp.

Maillard, C., and G. Soliman, 1986: Hydrography of the Red Sea and exchanges with the Indian Ocean in summer. *Oceanol. Acta,* **9,** 249–269.

Maxworthy, T., 1997: A frictionally and hydraulically constrained model of the convectively driven mean flow in partially enclosed seas. *Deep-Sea Res.,* **44,** 1339–1354.

Miller, A. R., 1964: Highest salinity in the World Ocean? *Nature,* **203,** 590.

Morcos, S. A., 1970: Physical and chemical oceanography of the Red Sea. *Oceanogr. Mar. Biol. Ann. Rev.,* **8,** 73–202.

Murray, S. P., and W. Johns, 1997: Direct observations of seasonal exchange through the Bab el Mandab Strait. *Geophys. Res. Lett.,* **24,** 2557–2560.

Neumann, J., 1952: Evaporation from the Red Sea. *Israel Explor. J.,* **2,** 153–162.

Ohmura, A., and H. Gligen, 1991: Global Energy Balance Archive (GEBA). World Climate Program—Water Project, A7, Rep. 2, GEBA Database, Interactive Appl. Retrieving Data, Verlag der Fachvereline, 60 pp.

Patzert, W. C., 1974: Volume and heat transports between the Red Sea and Gulf of Aden and notes on the Red Sea heat budget. *Symp. L'Oceanographie Physique de la Mer Rouge,* Paris, France, Association Internationale des Sciences Physiques de l'Ocean, 191–201.

Payne, R. E., 1972: Albedo of the sea surface. *J. Atmos. Sci.,* **29,** 959–970.

Privett, W. C., 1959: Monthly charts of evaporation from the North Indian Ocean, including the Red Sea and Persian Gulf. *Quart. J. Roy. Meteor. Soc.,* **85,** 424–428.

Reed, R. K., 1977: On estimating insolation over the oceans. *J. Phys. Oceanogr.,* **7,** 482–485.

Rosati, A., and K. Miyakoda, 1988: A general circulation model for the upper ocean circulation. *J. Phys. Oceanogr.,* **18,** 1601–1626.

Rossow, W. B., and Y.-C. Zhang, 1995: Calculation of surface and top-of-atmosphere radiative fluxes from physical quantities based on ISCCP data sets, II: Validation and first results. *J. Geophys. Res.,* **100,** 1167–1197.

Shapiro, G. I., and S. L. Meschanov, 1991: Distribution and spreading of Red Sea water and salt lens formation in the northwest Indian Ocean. *Deep-Sea Res.,* **38,** 21–34.

Siedler, G., 1968: Schichtungs- und Bewegungsverhaltnisse am Sudausgang des Roten Meeres. *Meteor. Forschungsergeb.,* **4,** 1–76.

Smeed, D., 1997: Seasonal variation of the flow in the strait of Bab el Mandab. *Oceanol. Acta,* **20,** 773–781.

Smith, S. D., 1988: Coefficients for sea surface wind stress, heat flux, and wind profiles as a function of wind speed and temperature. *J. Geophys. Res.,* **93,** 15 467–15 472.

——, 1989: Water vapor flux at the sea surface. *Bound.-Layer Meteor.,* **47,** 277–293.

Souvermezoglou, E., N. Metzl, and A. Poisson, 1989: Red Sea budgets of salinity, nutrients and carbon calculated in the Strait of Bab el Mandab during the summer and winter seasons. *J. Mar. Res.,* **47,** 441–456.

Stowe, L. L., A. M. Ignatov, and R. R. Singh, 1997: Development, validation, and potential enhancements to the second-generation operational aerosol product at the National Environmental Sat-

ellite Data and Information Service of the National Oceanic and Atmospheric Administration. *J. Geophys. Res.,* **102,** 16 923–16 934.

Tragou, E., and C. Garrett, 1997: The shallow thermohaline circulation of the Red Sea. *Deep-Sea Res.,* **44,** 1355–1376.

Van Aken, H. M., and L. Otto, 1974: Observations of the exchange of water in the Strait of Bab el Mandab in 1967. *Symp. L'Oceanographie Physique de la Mer Rouge,* Paris, France, Association Internationale des Sciences Physiques de l'Ocean, 229–252.

Vercelli, F., 1927: Campagne Idrografica della R. N. Amrairaglio Magnaghi in Mar Rosso 1923–1924. *Ann. Idrogr.,* **2,** 1–208, 267–290.

Verzhbitskiy, E. V., and A. A. Shreider, 1995: Seafloor spreading in the Red Sea–Gulf of Aden region from geomagnetic and geothermal data. *Oceanology,* **34,** 556–562.

Weare, B., 1989: Uncertainties in estimates of surface heat fluxes derived from marine reports over the tropical and subtropical oceans. *Tellus,* **41A,** 357–370.

Woelk, S., and D. Quadfasel, 1996: Renewal of deep water in the Red Sea during 1982–1987. *J. Geophys. Res.,* **101** (C8), 18 155–18 165.

Woodruff, S. D, R. J. Sleutz, R. L. Jenne, and P. M. Steurer, 1987: A comprehensive ocean–atmosphere data set. *Bull. Amer. Meteor. Soc.,* **68,** 1239–1250.

Yegorov, N. I., 1950: Calculation of the heat balance of the Red Sea. *Meteor. Gidrol.,* **3,** 49–56.

Zahariev, K., and C. Garrett, 1997: An apparent surface buoyancy flux associated with the nonlinearity of the equation of state. *J. Phys. Oceanogr.,* **27,** 362–368.

Zhang, Y. C., W. B. Rossow, and A. A. Lacis, 1995: Calculation of surface and top-of-atmosphere radiative fluxes from physical quantities based on ISCCP data sets. Part I: Method and sensitivity to input data uncertainties. *J. Geophys. Res.,* **100,** 1149–1165.